DOE/ET-53088-292 IFSR #292

Thermally Driven Convective Cells and Tokamak Edge Turbulence

D. R. Thayer and *P. H. Diamond*

Institute for Fusion Studies
The University of Texas at Austin
Austin, Texas 78712

July 1987

Thermally Driven Convective Cells and Tokamak Edge Turbulence

D. R. Thayer and P. H. Diamond

Institute for Fusion Studies, The University of Texas at Austin, Austin, Texas 78712

ABSTRACT

A unified theory for the dynamics of thermally driven convective cell turbulence is presented. The cells are excited by the combined effects of radiative cooling and resistivity gradient drive. The model also includes impurity dynamics. Parallel thermal and impurity flows enhanced by turbulent radial duffusion regulate and saturate overlapping cells, even in regimes dominated by thermal instability. Transport coefficients and fluctuation levels characteristic of the saturated turbulence are calculated. It is found that the impurity radiation increases transport coefficients for high density plasmas, while the parallel conduction damping, elevated by radial diffusion, in turn quenches the thermal instability. The enhancement due to radiative cooling provides a resolution to the dilemma of explaining the experimental obseration that potential fluctuations exceed density fluctuations in the edge plasma ($e\Phi/T_e > n/n_0$).

I. INTRODUCTION

It is well known that the study of tokamak edge turbulence is important since it can help in the development of an optimized design of limiters and divertors. The plasma edge is a boundary for the central plasma, thus its analysis is paramount in a global confinement study. Recent tokamak edge turbulence experiments indicate a high level of electrostatic potential ($e\Phi/T_e$) and density (n/n_0) fluctuations (10-50%) as well as the associated radial transport coefficients.[1-6] A detailed understanding of this highly turbulent saturated state may also prove invaluable for the exploitation of improved confinement regimes, such as the ASDEX H-mode, which maybe dependent on the edge fluctuations and induced transport for magnetic separatrix configurations.[7] Furthermore, since edge plasma diagnostics are quite good (the edge plasma is accessible to electrostatic and magnetic probes), it is also instructive to study edge turbulence in detail and make comparisons between the predictions of turbulence theories and experimental results.

In view of edge plasma parameters, the most widely accepted theoretical candidates for models of edge turbulence are resistivity gradient driven turbulence[8] and dissipative density gradient driven turbulence theory.[9] Here, we focus on the stronger candidate, resistivity gradient driven turbulence theory. The linear antecedent of this turbulence theory is the rippling mode.[10] At present, the resistivity gradient driven turbulence theory[11,12,13] and a resitivity-impurity[14] gradient driven turbulence theory[15] have recieved substantial but still incomplete success in explaining the plasma edge fluctuation and transport characteristics.

The basic model of resisitivity gradient driven turbulence incorporates the parallel Ohm's law, the vorticity equation, and a resistivity (or temperature) evolution equation for the electrostatic potential (ϕ), resistivity (η), and parallel current (J_z) fluctuations. The linear eigenmodes for potential and resistivity which are determined from this model are skewed to one side of the mode rational surface (about which the current fluctuation is centered). In the nonlinear turbulent state, this asymmetry is accentuated so that the current fluctuations decouple from the potential and resistivity fluctuations.[11] It should be noted that this decoupling of the current fluctuation is similar to that which is assumed for the current convective

instability.[16] As a result, the vorticity equation is eliminated from the analysis, so that the Ohm's law and resistivity equation can be combined into a nonlinear equation for the saturated turbulent state. The essential features of the saturated turbulent state are embodied in the cross-field diffusion coefficient, D_T, which represents the radial $\mathbf{E}\times\mathbf{B}$ turbulent convection, and the turbulently enhanced characteristic radial scale, Δ_T, which lead to an increased parallel thermal conduction. This is seen in the schematic representation of the steady state resistivity fluctuation equation, $(\chi_T k_{\|}'^2\Delta_T^2 - D_T\partial^2/\partial x^2)\eta = (E_0 L_S/B_z L_\eta x)\eta$. The nonlinear saturated state results from a balance between the resistivity gradient drive and the parallel thermal conduction damping.

One of the successes of the basic resistivity gradient driven turbulence theory is that the diffusion coeficient, $D_{T\,k} \propto (\chi_T k_{\|}'^{\,2})^{-1/3}$, is weakly dependent on the parallel thermal conduction, χ_T, so that the saturation value tends to be on the order of experimental values. The predictions for potential ($e\Phi/T_e \approx .1$) and density fluctuations ($n/n_0 \approx .2$), as well as the radial particle diffusion coefficient ($D_n \approx 10^4 cm^2/sec$), are on the order of, but slightly less than the experimental values. One of the failures of the theory is that it predicts that the potential fluctuations are smaller than the density fluctuations ($e\Phi/T_e < n/n_0$), which is contrary to the experimental observations.[4]

In order to resolve some of the shortcomings of the resisitivity gradient driven turbulence model, it is necessary to include other dominant physical processes in the model. To this end, we address the important effect of impurity radiation in the edge plasma.[17] Currently, there exists conclusive experimental evidence that radiation from low ionization states of low Z impurities in the plasma edge is significant (on the order of the input power) and is manifested in terms of MARFE activity[18] or the mature detached plasma state[19]. The low temperature edge plasma typically contains a moderate impurity density (approximately 1% of the edge density) which exhibits a

large impurity radiation rate ($I_Z/T_0 \approx 10^{-9} cm^3/sec$).

The MARFE phenomena has been theoretically described as a thermal instability.[20,21] This instability is understood by including an impurity radiation cooling term, proportional to the impurity density, the edge density, and the radiation rate ($n_z n I_Z$), in the temperature equation. Typically, the carbon C-IV impurity state is considered and the radiation rate slope as a function of temperature is negative ($dI_Z/dT<0$) for the low temperatures in the edge plasma. The thermal instability evolves by considering a negative temperature perturbation which increases the radiation cooling due to a differential increase in the radiation rate and an additive differential increase in the edge density (assuming parallel sound wave propagation leads to a constant pressure, nT=const.). The temperature is consequently decreased further so that the thermal instability is apparent. The basic thermal instability growth rate (including the thermal conduction damping) is $\gamma_{thermal}=\gamma_{rad}-\gamma_{cond} \approx (2n_Z/3)[2(I_Z/T)-(dI_Z/dT)]-\chi_T k_{||}^2$. From this growth rate expression it is clear that a marginal stability occurs when the radiative cooling drive balances the parallel thermal conduction damping, $\gamma_{rad} \approx \gamma_{cond}$. Recently, this instability has been renamed the "thermal condensation instability"[22] in order to emphasize the role of density perturbations in the thermal instability. However, both the destabilizing effects from the gradient of the radiation rate and the perturbation of the density are typically of the same order. It should also be noted that the thermal instability growth rate is sizeable, and it is greater than or equal to the resistivity gradient driven mode growth rate in high density tokamak edge plasmas. However, it is difficult to envision an edge turbulence model based exclusively on thermal instability. Indeed, a major limitation of an edge turbulence model which is based solely on the thermal instability is that it does not address the crucial issue of cross-field transport. If the turbulent radial flow enhancement of the parallel conduction damping is neglected, then the saturation level predictions will be far too high. Consequently, it is natural to include the important features from both theories in a complete theory of edge turbulence.

The primary scope of this work is the derivation of an analytic theory for thermally driven convective cell turbulence which allows consistent predictions of

radial transport coefficients. To this end, the thermal instability, driven by impurity radiative cooling, is coupled to resistivity and impurity gradient driven turbulence. This model of edge turbulence incorporates the destabilizing effects of resistivity and impurity gradient drive with impurity radiation drive, as well as the stabilizing effects of parallel thermal conduction and parallel impurity flows. The essential feature of a turbulent cross-field transport is included throughout the analysis. Consequently, the marginal stability condition for the thermal instability is significantly affected by radial turbulent convective cell enhancement of the parallel thermal and impurity conduction damping.

The principle results of the analysis presented here is summarized in the following.

(i) A theory for thermally driven convective cell turbulence has been developed as a unified model of resistivity gradient driven turbulence and the thermal instability. The fundamental result is that the saturation fluctuation levels and cross-field transport are enhanced due to the impurity radiative cooling, while the turbulently elevated parallel conduction in turn regulates the thermal instability.

(ii) For high density machines (such as Alcator), the impurity radiation can lead to an order of magnitude enhancement in saturation fluctuation levels and transport coefficients. Alternativley, for these radiation dominated cases, the structure of the resultant diffusion coefficient is altered to include a strong dependence on the parallel conduction, $D_T \propto \gamma_{rad}^2 (\chi_T k_{||}'^2)^{-1}$. Thus, the convective cell turbulence tends to quench the thermal instability at a well defined, finite level. The saturation analysis indicates a smooth connection from weak impurity radiation conditions to radiation dominated situations. Calculations also indicate that the impurity radiation enhanced radial particle diffusion coefficient is close to experimental values ($D_n > 10^4 cm^2/sec$). Estimates for the value of the magnetic fluctuation induced radial thermal conduction indicate that it is just one percent of the value of radial particle diffusion.

(iii) The fluctuation saturation levels have been found to be sizeably increased (above the no impurity radiation situation) up to values on the order of experimental measurements. The saturation levels are also determined to be sensitive to the

particular operating parameters considered. Consequently, the fluctuation saturation levels have been calculated as a function of the radiation rate. One of the more interesting results of the analysis presented here is that the nonlinear structure responsible for the impurity radiation enhancement of the potential and density fluctuations tends to force the potential fluctuation to be greater than the density fluctuation at saturation ($e\Phi/T_e > n/n_0$), which is in agreement with experiment[4]. This is a consequence of the weak scaling of the density ($n/n_0 \sim \Delta/L \sim D^{1/4}$) and the strong scaling of the potential fluctuations with the diffusion coefficient ($e\Phi/T_e \sim D^{3/4}$).

(iv) It is proposed that the impurity radiation enhancement of the fluctuation levels at saturation might be responsible for the observed particle confinement time (τ_p) roll-over[6] at high density (n). It is also pointed out that the particle diffusion coefficent has a reduces sensitivity to a scaling with the loop voltage (V_L, $E_0 \sim V_L/2\pi R_0$).

The remainder of this article is organized in the following manner. Section II contains the basic theoretical model of thermally driven convective cell turbulence. Section III contains a heuristic derivation of the thermally driven convective cell analysis which encompasses the thermal instability and the resistivity-impurity gradient driven turbulence analysis. In Sec. IV, the linear theory is presented. In Sec. V, we present the nonlinear theory as well as the saturation fluctuation levels and transport coefficient predictions for tokamak parameters. Finally, our discussion and summary of the results are presented in Section VI.

II. THEORETICAL MODEL

The theoretical model of thermally driven convective cell turbulence encompasses the reduced resistive magnetohydrodynamic (MHD) equations in cylindrical geometry[23], a resistivity evolution equation containing impurity radiation sources, and an impurity dynamics equation for a single low-Z impurity species. In the electrostatic approximation, the potential (ϕ), resistivity (η), and parallel current (J_z) fluctuations are coupled through the parallel Ohm's law, and parallel vorticity equations, respectively,

$$-B_z \nabla_{\parallel} \tilde{\phi} = \tilde{\eta} J_{z0} + \eta_0 \tilde{J}_z, \tag{1}$$

and

$$\rho_m \frac{d}{dt} \nabla_{\perp}^2 \tilde{\phi} = B_z \nabla_{\parallel} \tilde{J}_z. \tag{2}$$

Here, B_z is the toroidal magnetic field, ρ_m is the mass density, $\phi = \Phi / B_z$ is the electrostatic potential normalized to the magnetic field, $d/dt = \partial/\partial t + \mathbf{v_r} \cdot \nabla = \partial/\partial t - (\nabla_{\perp} \phi \times \mathbf{b}) \cdot \nabla$ is the $\mathbf{E} \times \mathbf{B}$ convective derivative, $\nabla_{\parallel}$ is the parallel derivative along the magnetic field, $\nabla_{\perp}$ is the perpendicular derivative, and $\mathbf{b}$ is the unit vector along the magnetic field. The subscript 0 denotes average quantities, bold face quantities are vectors, and the tilde (~) represents perturbed quantities.

The temperature equation which contains the effects of the impurity radiation cooling is

$$\frac{3}{2} n \frac{d}{dt} T = \kappa_T \nabla_{\parallel}^2 T - n n_Z I_Z(T) + H \, . \tag{3}$$

Here, n_Z is the impurity density, n is the electron density, I_Z is the impurity radiation rate, κ_T is the parallel thermal conductivity, T is the temperature, and H represents the heat source. The temperature equation, Eq. (3), is used to obtain a Spitzer resistivity evolution equation, where the resistivity relation is $\eta = Z_{eff} \eta_{sp}$, the Spitzer

resistivity is $\eta_{sp} \propto T^{-3/2}$, and the effective ion charge for a single impurity species with charge state Z is $Z_{eff}=\Sigma n_i Z_i^2/n_0 \approx 1+Z^2 n_Z/n_0$. After expanding the resistivity equation about the average values ($H=n_0 n_{Z0} I_Z(T_0)$, T_0, η_{sp0}, Z_{eff0}, n_0, n_{Z0}), the resistivity fluctuation equation is

$$\left(\frac{d}{dt}-\chi_T\nabla_{\|}^2-\gamma_R\right)\tilde{\eta}_{SP}=\frac{1}{r}\frac{\partial\tilde{\phi}}{\partial\theta}\frac{d\eta_{SP0}}{dr}+\gamma_Z\frac{\eta_{SP0}}{Z_{eff0}}\tilde{Z}_{eff}. \tag{4}$$

Here, $\chi_T=2\kappa_T/3n$ is the normalized parallel thermal conduction, and the radiation source (growth) rates (γ_R and γ_Z) are defined by

$$\gamma_R=\frac{2}{3}n_{Z0}\left[\frac{I_Z(T_0)}{T_0}-\frac{dI_Z(T_0)}{dT_0}\right], \tag{5}$$

and

$$\gamma_Z=Z_{eff0}\frac{n_0}{Z^2}\frac{I_Z(T_0)}{T_0}=\left(\frac{n_0}{Z^2}+n_{Z0}\right)\frac{I_Z(T_0)}{T_0}, \tag{6}$$

where constant pressure (nT) has been assumed, since it is maintained by parallel sound wave propagation[14,15]. In the above expressions, the impurity dynamics have been accounted for by the effective Z (Z_{eff}) fluctuation which results in an additional radiation rate term (γ_Z). This term is proportional to the edge density and the impurity radiation rate, and it is on the order of the fundamental radiation rate term (γ_R).

The impurity dynamics equation, which closes the set of equations for thermally driven convective cells, has been derived by Rutherford[14,15]

$$\left(\frac{d}{dt}-\chi_Z\nabla_{\|}^2\right)\tilde{Z}_{eff}=\frac{1}{r}\frac{\partial\tilde{\phi}}{\partial\theta}\frac{dZ_{eff0}}{dr}. \tag{7}$$

This equation is derived from the continuity equations for impurity and hydrogenic ion density along with the parallel velocity equations. The parallel diffusion

operator ($\chi_Z \nabla_{||}^2$) is a result of the balance between parallel impurity pressure gradient and impurity-ion friction. The Z_{eff} fluctuation equation, Eq. (7), is derived in the limit of a single low Z impurity species where $n_Z Z << n_i \approx n_e$ and $n_Z Z^2 \approx n_i$. It should be noted that the parallel impurity conductivity, χ_Z, is much less than the parallel thermal conductivity, χ_T, ($\chi_Z = \upsilon_i^2/Z^2\nu_{ii} << \chi_T$, $\chi_Z/\chi_T \approx .025$).

The linear and nonlinear theory of the thermally driven convective cell turbulence is embodied in the parallel Ohm's law, Eq. (1), the parallel vorticity equation, Eq. (2), the resistivity fluctuation equation, Eq. (4), and the impurity dynamics equation, Eq. (7). This set of coupled equations forms a complete system for the potential (ϕ), resistivity (η), and parallel current (J_z) fluctuations.

III. HEURISTICS OF THERMALLY DRIVEN CONVECTIVE CELL TURBULENCE

In order to gain insight into the dynamics of thermally driven convective cell turbulence, it is instructive to consider heuristic discussions of a simplified model containing the essential elements of the thermal and resistivity gradient driven instability mechanisms. Special attention is focused on the role of coupled cross-field and parallel transport processes in regulating the turbulence characteristics.

A minimal representation of thermally driven convective cells is contained in reduced forms of the temperature and Ohm's law equations:

$$\frac{d\tilde{T}}{dt} - \chi_T \nabla_{||}^2 \tilde{T} = -\tilde{v}_r \frac{dT_0}{dr} + \gamma_R \tilde{T} , \tag{8}$$

and

$$E_0 \left(\frac{1}{\eta_0} \frac{d\eta_0}{dT} \right) \tilde{T} = -B_z \nabla_{||} \tilde{\phi} . \tag{9}$$

Here, $E_0 = \eta_0 J_{z0}$ and impurity dynamics have been ignored for simplicity. Renormalizing the convective nonlinearity of Eq. (8) as a turbulent radial diffusion operator and combining Eqs. (8), and (9) yields:

$$\left(\frac{\partial}{\partial t} + \chi_T k_{||}^2 - D_{Tk} \frac{\partial^2}{\partial x^2} \right) \tilde{T}_k = \left(\gamma_R + \frac{E_0}{B_z} L_\eta^{-1} \frac{k_\theta}{k_{||}} \right) \tilde{T}_k . \tag{10}$$

In the above equation, $D_{T\,k}$ accounts for the effects of overlapping nonlinearly interacting cell flows on the evolution of the mode ($\mathbf{k}$), and $L_\eta^{-1} = (1/\eta_0)(d\eta_0/dT)(dT_0/dr)$. Equation (10) constitutes the simplest possible model of thermally driven convective cell turbulence, and is operationally equivalent to the model of current convective turbulence[16] with radiative enhancement. This simplification is possible because the $k_{||} \to 0$ singularity at the $\mathbf{k} \cdot \mathbf{B}$ resonant surface is resolved by nonlinearity (turbulent diffusion). Hence, the associated current perturbation (J) can be ignored, so that the rippling mode reverts to its electrostatic

antecedent, the current convective instability.

The characteristic radial cell size is determined by the asymptotic balance of parallel thermal conduction $\chi_T k_\theta^2 x^2/L_S^2$ with turbulent radial diffusion $D_{Tk}\partial^2/\partial x^2$, and is given by:

$$\Delta_{Tk} = \left(\frac{L_S^2 D_{Tk}}{\chi_T k_\theta^2} \right)^{1/4} . \tag{11}$$

Note that Δ_{Tk} is nonlinear in the fluctuating electric field amplitude, via its dependence on D_{Tk}. Saturated stationary turbulence ($\partial/\partial t \to 0$) occurs when the cell size (Δ_{Tk}) adjusts so that radiative and resistivity gradient driven energy production is balanced by thermal conduction dissipation. Proceeding schematically by taking $k_{||} \to k_\theta \Delta_{Tk}/L_S$, it is easily seen that the requisite value of Δ_{Tk} can be obtained by the solution of

$$\gamma_R + \left(\frac{E_0}{B_z} \frac{L_S}{L_\eta} \right) \Delta_{Tk}^{-1} - \left(\frac{\chi_T k_\theta^2}{L_S^2} \right) \Delta_{Tk}^2 = 0 . \tag{12}$$

Equation (12) constitutes the nonlinear saturation condition for thermally driven convective cell turbulence. Various limiting cases are now examined. First, in the limit $\gamma_R \to 0$, the previously derived expression for resistivity gradient driven turbulence,

$$D_{Tk} = \left(\frac{L_S}{L_\eta} \frac{E_0}{B_z} \right)^{4/3} \left(\frac{L_S^2}{k_\theta^2 \chi_T} \right)^{1/3} , \tag{13}$$

is straightforwardly recovered. Second, in the opposite (radiation dominated) limit, where $\gamma_R > (E_0/B_z)(L_S/L_\eta)\Delta_{Tk}^{-1}$ [Δ_{Tk} is to be evaluated using Eq. (13)], Eq. (12) predicts that

$$D_{Tk} = \frac{\gamma_R^2 L_S^2}{\chi_T k_\theta^2}. \qquad (14)$$

Note that $D_{T\,k}$ as given by Eq. (14) exhibits strong T_0 and q(r) dependence, i.e. $D \sim \gamma_R{}^2 q^2(r)/(s^2 T_0{}^{5/2})$. Here $s = R_0 q(r)/L_S$. Finally, it is clear that in intermediate regimes, radiative effects enhance transport due to resistivity gradient driven turbulence. Hence, it is, perhaps, more useful to envision a unified model of thermally driven convective cell turbulence.

It is worthwhile to comment on the role of radial and parallel transport in regulating the thermal instability driven by radiative cooling (γ_R). It is well known that radial excursions mediated by the convection cell flows enhance the dissipative effects of parallel thermal conduction. The two combined effects result in the damping decrement $\gamma_{d\,k} = -(k_\theta{}^2/L_S{}^2)\Delta_{T\,k}{}^2 \chi_T = -(k_\theta/L_S)\,(D_{T\,k}\chi_T)^{1/2}$ which appears in Eq. (12). Hence, radial transport also acts to increase the flow of heat along field lines and thus naturally offsets the effects of radiative cooling, γ_R. Thermal instability is thus quenched at a well defined, finite level, as shown in Eq. (14). By way of contrast, quasilinear analyses which ignore the effects of self-consistent radial transport predict unphysically large fluctuation levels independent of χ_T, $T/T_0 \sim 1$.

IV. LINEAR THEORY

In this section, the linear theory of thermally driven convective cells in tokamak edge plasmas is discussed. These cells are driven by the coupling of the resistivity-impurity gradient driven instability to the thermal instability. A single linear equation for the electrostatic potential fluctuation is obtained by combining Ohm's law, Eq. (1), the vorticity equation, Eq. (2), the resistivity evolution equation, Eq. (4), and the impurity dynamics equation, Eq. (7),

$$\left\{ \left(\frac{\partial}{\partial t}-\chi_Z\nabla_{\|}^2\right)\left(\frac{\partial}{\partial t}-\chi_T\nabla_{\|}^2-\gamma_R\right)\left(\frac{\rho_m}{B_z^2}\frac{\partial}{\partial t}\nabla_{\perp}^2+\frac{1}{\eta_0}\nabla_{\|}^2\right) \right.$$

$$\left. +\frac{J_{z0}}{B_z}\left(\frac{L_\eta+L_Z}{L_\eta L_Z}\right)\left[\frac{\partial}{\partial t}-\left(\frac{L_\eta\chi_T+L_Z\chi_Z}{L_\eta+L_Z}\right)\nabla_{\|}^2-\left(\frac{L_\eta}{L_\eta+L_Z}\right)\left(\gamma_R-\gamma_Z\right)\right]\frac{1}{r}\frac{\partial}{\partial\theta}\nabla_{\|} \right\} \tilde{\phi}=0 . \qquad (15)$$

Here, the resistivity scale length is $L_\eta=[d(\ln\eta_0)/dr]^{-1}$, the Z_{eff} scale length is $L_Z=[d(\ln Z_{eff0})/dr]^{-1}$, while the average resistivity, $\eta_0=Z_{eff0}\eta_{sp0}$, and the resistivity fluctuations,

$$\tilde{\eta}=\tilde{Z}_{eff}\,\eta_{sp0}+Z_{eff0}\tilde{\eta}_{sp} \quad , \qquad (16)$$

are used in Eq. (1).

The linear equation for the potential fluctuation, Eq. (15), is solved for an eigenmode perturbation of the form $\phi=\phi(x)\exp[\gamma t+i(n\varphi-m\theta)]$. The parallel wave vector is $k_{\|}=k_{\|}'\,x$, $k_{\|}'=k_\theta/L_S$, $k_\theta=m/r_S$, $x=r-r_S$, $q(r_S)=m/n$, m is the poloidal mode number, n is the toroidal mode number, r_S is the radial mode rational surface position, $L_S=R_0q^2/r_Sq'$ is the shear scale length, q is the safety factor, and R_0 is the major radius. After making the following operator transformations, $\nabla_{\|}\rightarrow ik_{\|}=ik_{\|}'x$, $\nabla_{\perp}^2\rightarrow d^2/dx^2$, $\partial/r\partial\theta\rightarrow -ik_\theta$, and $\partial/\partial t\rightarrow\gamma$, the radial second order differential eigenmode equation for the potential is

$$\left[\frac{d^2}{dX^2}-\left(\frac{1}{4}X^2-\frac{\delta_T}{2}\frac{X}{1+b_TX^2}-\frac{\delta_Z}{2}\frac{X}{1+b_ZX^2}\right)\right]\phi(X)=0\,. \tag{17}$$

The radial coordinate about the mode rational surface, $X=x/x_R$, is normalized with respect to a resistive layer width,

$$x_R=\left[\gamma\left(\frac{\mu_0\rho_m}{B_z^2}\right)\frac{\eta_0}{\mu_0}\frac{L_S^2r_S^2}{4m^2}\right]^{1/4}. \tag{18}$$

In Eq. (17), the resistivity gradient drive parameter is

$$\delta_T=\frac{L_S}{L_\eta}\frac{\eta_0J_{z0}}{B_z}\frac{1}{2\left(\gamma-\gamma_R\right)x_R}\left\{1+\frac{L_\eta}{L_Z}\frac{\gamma_Z\chi_T}{\left[\gamma\left(\chi_T-\chi_Z\right)+\gamma_R\chi_Z\right]}\right\}, \tag{19}$$

the impurity gradient drive parameter is

$$\delta_Z=\frac{L_S}{L_Z}\frac{\eta_0J_{z0}}{B_z}\frac{1}{2\gamma x_R}\left\{1-\frac{\gamma_Z\chi_Z}{\left[\gamma\left(\chi_T-\chi_Z\right)+\gamma_R\chi_Z\right]}\right\}, \tag{20}$$

the thermal conduction damping parameter is

$$b_T=\frac{\chi_Tm^2x_R^2}{r_S^2L_S^2(\gamma-\gamma_R)}, \tag{21}$$

and the impurity conduction damping parameter is

$$b_Z=\frac{\chi_Zm^2x_R^2}{r_S^2L_S^2\,\gamma}\,. \tag{22}$$

In general, the eigenmode equation, Eq. (17), can be approximately solved using the WKB method. The eigenfunctions are skewed to one side of the mode rational surface ($X=0$) due to the gradient destabilizing terms (δ_T and δ_Z). The growth rate of the thermally driven convective cell can be obtained using a WKB connection or phase quantization condition,

$$\int_0^{X_0} dX \left(\frac{\delta_T}{2} \frac{X}{1+b_T X^2} + \frac{\delta_Z}{2} \frac{X}{1+b_Z X^2} - \frac{1}{4} X^2 \right)^{1/2} = \frac{\pi}{2} + l\pi ; \quad l = 0, 1, 2, \ldots, \tag{23}$$

where the turning point is

$$X_0 = \frac{2\delta_T}{1+b_T X_0^2} + \frac{2\delta_Z}{1+b_Z X_0^2} . \tag{24}$$

The eigenmode equation, Eq. (17), can be easily solved in several limits[12]. For the case of small parallel conduction ($\chi_Z << \chi_T \to 0$ or b_Z, $b_T \to 0$), the eigenmode is expressed in terms of a simple Guassian-Hermite polynomial solution, where the dominant mode (H_0=1) is

$$\phi(X) = \phi_0 \exp\left[-(X-\delta)^2/4 \right], \tag{25}$$

and the growth rate ($\delta = \delta_T + \delta_Z = 2^{1/2}$) is

$$\frac{\gamma}{\gamma_0} = \left\{ \frac{1 + \eta_Z \left[1 + \left(\frac{\gamma_Z}{\gamma_0} - \frac{\gamma_R}{\gamma_0} \right) \left(\frac{\gamma}{\gamma_0} \right)^{-1} \right]}{1 - \frac{\gamma_R}{\gamma_0} \left(\frac{\gamma}{\gamma_0} \right)^{-1}} \right\}^{4/5} . \tag{26}$$

Here, the ratio of resistivity to impurity scale length is η_Z ($\eta_Z = L_\eta / L_Z$), and the basic growth rate of the rippling mode[11] (only resistivity gradient driven, no impurity gradient or radiation) is

$$\gamma_0 = \left(\frac{\eta_0^3 J_{z0}^4 L_S^2 m^2}{16 B_Z^2 L_\eta^4 \rho_m r_S^2} \right)^{1/5} . \tag{27}$$

It should be noted that the resonance denominator in Eq. (26) forces the growth rate to exceed the radiation rate ($\gamma > \gamma_R$) so that no singularity occurs. Also, typically $\gamma_Z > \gamma_R$,

so that there is an enhancement due to the $\gamma_Z - \gamma_R$ term in the numerator. For the case of the impurity scale length being much longer than the resistivity scale length ($\eta_Z \rightarrow 0$), the growth rate is[17]

$$\frac{\gamma}{\gamma_0} = \frac{1}{\left[1 - \frac{\gamma_R}{\gamma_0}\left(\frac{\gamma}{\gamma_0}\right)^{-1}\right]^{4/5}} \quad . \tag{28}$$

It is clear from Eq. (28) that the radiative cooling enhancement of the instability is sizeable for γ_R on the order of γ_0 (for $\gamma_R \approx \gamma_0 \Rightarrow \gamma > \gamma_0$, and if $\gamma_R/\gamma_0 = 1.0$, then $\gamma/\gamma_0 \approx 1.9$). In the radiation dominated limit ($\gamma_R >> \gamma_0$), the growth rate closely tracks γ_R (if $\gamma_R/\gamma_0 = 10.0$, then $\gamma/\gamma_0 \approx 10.6$).

In the large parallel conduction limit ($bX^2 >> 1$), the growth rate can be obtained by an approximate evaluation of the WKB phase quantization integral, Eq. (23).[11] Here, the parallel conduction parameter (b) represents the thermal conduction (b_T) for the case when impurity gradients are neglected, or it represents the impurity conduction (b_Z) for the case of an isothermal limit ($b_T \rightarrow \infty$). In the large conduction limit, the growth rate is sharply reduced as $\gamma \propto \chi^{-4/3}$.

The linear eigenmode equation for thermally driven convective cells, Eq. (17), has been extensively studied using a shooting code solution. To this end, it is convenient to express the normalized growth rate solution (γ/γ_0) in terms of five noramalized parameters (γ_R/γ_0, γ_Z/γ_0, η_Z, χ_Z/χ_T, and $C = \chi_T m^2 x_{R0}^2/\gamma_0 r_S^2 L_S^2$ for $x_{R0} = x_R$ at $\gamma = \gamma_0$). As stated above, for a large normalized thermal conduction parameter ($C > 1.$), the normalized growth rate is sizeably reduced for the case of no radiation enhancement ($C = 10$; γ_R/γ_0, γ_Z/γ_0, η_Z, $\chi_Z/\chi_T \rightarrow 0$; $\Rightarrow \gamma/\gamma_0 = 0.039$). However, if a finite

radiation rate ($\gamma_R/\gamma_0 \sim 1$) is included in the analysis, then the growth rate will be reduced no less than the radiation rate ($\gamma/\gamma_0 \sim 1$).

At the end of the nonlinear theory section, Sec. V., detailed comparisons of the predictions from the thermally driven convective cell turbulence theory are presented for a low density tokamak (Text) and a high density tokamak (Alcator). The typical Text parameters, displayed in the next section (Table I), are used in the shooting code to determine the typical linear electrostatic potential eigenmode structure. In Fig. 1(a), the eigenfunction for Text parameters is shown skewed about the mode rational surface ($x/x_R = 0$). In Fig. 1(b), the eigenfunction for Text parameters with a large enhancement in the radiation rate is displayed which shows a very similar structure to the unenhanced mode. In Fig. 2, the growth rate for Text parameters is plotted as a function of the radiation rate. The growth rate enhancement is found to be linear in the radiation rate, which is consistent with the large radiation limit, as mentioned above.

V. NONLINEAR THEORY

The nonlinear theory of thermally driven convective cells in tokamak edge turbulence is derived in this section. The instability, driven by resistivity and impurity gradients and by impurity radiative cooling, is saturated by turbulently enhanced parallel thermal and impurity conduction. The coupling of parallel transport with turbulent radial diffusion is crucial. Expressions for nonlinear fluctuation saturation levels and radial transport quantities are derived. In general, the resistivity gradient driven fluctuation levels are enhanced by radiation, but still limited by parallel transport processes. Also, evaluations for typical low density (Text) and high density (Alcator) tokamak parameters are presented.

The derivation of the equations for the nonlinear saturated state follow that of Refs. (11) and (15). In the turbulent saturated state, the current fluctuation, J_z, which is centered about the mode rational surface, decouples from the potential, ϕ, resistivity, η_{sp}, and impurity fluctuations, Z_{eff}, which are shifted away from the rational surface. With the elimination of the vorticity equation, Eq. (2), the rippling system reverts to that characteristic of the current convective instability.[16] Thus, Ohm's law, Eq. (1), can be incorporated in the resistivity equation, Eq.(4), and the impurity dynamics equation, Eq.(7). After the $\mathbf{E}\times\mathbf{B}$ convective derivatives have been renormalized in terms of radial diffusion operators,[11] a set of coupled equations for η_{sp} and Z_{eff} in the nonlinear saturated state are given by

$$\left(\chi_T k_{\|}'^2 x^2 - \gamma_R - D_{T\,k}\frac{d^2}{dx^2}\right)\frac{\tilde{\eta}_{sp\,k}(x)}{\eta_{sp0}} = \frac{J_{z0}L_S\eta_0}{B_z L_\eta x}\left(\frac{\tilde{\eta}_{sp\,k}(x)}{\eta_{sp0}} + \frac{\tilde{Z}_{eff\,k}(x)}{Z_{eff0}}\right) + \gamma_Z\frac{\tilde{Z}_{eff\,k}(x)}{Z_{eff0}}, \qquad (29)$$

and

$$\left(\chi_Z k_{\|}'^2 x^2 - D_{Z\,k}\frac{d^2}{dx^2}\right)\frac{\tilde{Z}_{eff\,k}(x)}{Z_{eff\,0}} = \frac{J_{z0}L_S\eta_0}{B_z L_Z x}\left(\frac{\tilde{\eta}_{sp\,k}(x)}{\eta_{sp0}} + \frac{\tilde{Z}_{eff\,k}(x)}{Z_{eff0}}\right). \qquad (30)$$

In the above equations, the radial turbulent convective diffusion coefficients for resisitivity, D_T, and impurities, D_Z, are defined by

$$D_{T\,k} = \sum_{k''} k_{\theta}^{''2} \left| \tilde{\phi}_{k''} \right|^2 \left[\gamma_{k+k''} + \chi_T \left(k_{\|} + k_{\|}^{''} \right)^2 \right]^{-1} , \tag{31}$$

and

$$D_{Z\,k} = \sum_{k''} k_{\theta}^{''2} \left| \tilde{\phi}_{k''} \right|^2 \left[\gamma_{k+k''} + \chi_Z \left(k_{\|} + k_{\|}^{''} \right)^2 \right]^{-1} . \tag{32}$$

In order to obtain an approximate solution for the coupled equations, Eqs. (29) and (30), describing the saturated state, it is advantageous to first discuss the nonlinear radial scale lengths. In Eqs. (29) and (30), the turbulently enhanced parallel conduction and the radial diffusion are asymptotically balanced to determine the nonlinear scale lengths for resistivity, $\Delta_{T\,k}$, and impurity, $\Delta_{Z\,k}$, fluctuations,

$$\Delta_{T\,k} = \left(\frac{D_{T\,k}}{\chi_T k_{\|}^{'2}} \right)^{1/4} , \text{ and } \Delta_{Z\,k} = \left(\frac{D_{Z\,k}}{\chi_Z k_{\|}^{'2}} \right)^{1/4} . \tag{33}$$

A comparison between the average turbulent scale lengths, Δ_T and Δ_Z, can be made by writing the diffusion coefficients, D_T and D_Z, in terms of the average turbulent radial velocity, $v_r^2 = \Sigma_k k_\theta^2 |\phi_k|^2$, so that $D_T = v_r^2/\chi_T k_{\|}'^2 \Delta_T^2$ and $D_Z = v_r^2/\chi_Z k_{\|}'^2 \Delta_Z^2$. It then follows that the average scale lengths are

$$\Delta_T^3 = \frac{v_r}{\chi_T k_{\|}^{'2}} , \text{ and } \Delta_Z^3 = \frac{v_r}{\chi_Z k_{\|}^{'2}} , \tag{34}$$

while the radial diffusion coefficients are

$$D_T = \frac{v_r^{4/3}}{\left(\chi_T k_{\|}^{'2} \right)^{1/3}} , \text{ and } D_Z = \frac{v_r^{4/3}}{\left(\chi_Z k_{\|}^{'2} \right)^{1/3}} , \tag{35}$$

which implies that the ratio of the resistivity to the impurity scale length is small, $\Delta_T/\Delta_Z = (\chi_Z/\chi_T)^{1/3} < 1$. It should be noted that throughout this analysis the average

parallel wave vector, $k_{||}$, is dominated by the low m mode numbers, which has been validated by three-dimensional multiple-helicity numerical studies[11].

The saturated turbulent state for the simplified problem, with no impurity dynamics, can be represented in terms of a second order differential eigenmode equation. This calculation has been previously presented and is contained in Ref. 17. Here, where we have included the impurity dyanamics, instead of attacking the resultant fourth order equation, derived from Eqs. (29) and (30), we approximate the solution of the saturated state by using a moment technique which utilizes the scale disparity ($\Delta_T < \Delta_Z$). The moment equations of Eqs. (29) and (30) are obtained by multiplication by the Z_{eff} fluctuations and integration over the radial coordinate,

$$\left\langle \frac{\tilde{Z}}{Z_0} \middle| L_1 \middle| \frac{\tilde{\eta}}{\eta_0} \right\rangle + \left\langle \frac{\tilde{Z}}{Z_0} \middle| L_2 \middle| \frac{\tilde{Z}}{Z_0} \right\rangle = 0 , \tag{36}$$

and

$$\left\langle \frac{\tilde{Z}}{Z_0} \middle| L_3 \middle| \frac{\tilde{\eta}}{\eta_0} \right\rangle + \left\langle \frac{\tilde{Z}}{Z_0} \middle| L_4 \middle| \frac{\tilde{Z}}{Z_0} \right\rangle = 0 . \tag{37}$$

The moments in the above equations are defined by $\langle a|L|b\rangle = \int dx\, a^* L b$, while the operators are:

$$L_1 = \chi_T k_{||}'^2 x^2 - \gamma_R - D_T \frac{d^2}{dx^2} - \frac{L_S J_{z0} \eta_0}{L_\eta B_z x} \ , \ L_2 = -\frac{L_S J_{z0} \eta_0}{L_\eta B_z x} - \gamma_Z , \tag{38}$$

$$L_3 = -\frac{L_S J_{z0} \eta_0}{L_Z B_z x} , \text{ and } L_4 = \chi_Z k_{||}'^2 x^2 - D_Z \frac{d^2}{dx^2} - \frac{L_S J_{z0} \eta_0}{L_Z B_z x} . \tag{39}$$

The moment integrals in Eqs. (36) and (37) can be approximately evaluated in terms of the scale lengths, Δ_T and Δ_Z. After employing the scale disparity, the nontrivial solution of the coupled set of algebraic equations, Eqs. (36) and (37), is represented in terms of the zero of the determinant,

$$\begin{vmatrix} \left(\chi_T k_{\|}'^2 \Delta_T^2 - \gamma_R - \frac{L_S J_{z0} \eta_0}{L_\eta B_z \Delta_T}\right) & \left(-\frac{L_S J_{z0} \eta_0}{L_\eta B_z \Delta_Z} - \gamma_Z\right) \\ \left(-\frac{L_S J_{z0} \eta_0}{L_Z B_z \Delta_T}\right) & \left(\chi_Z k_{\|}'^2 \Delta_Z^2 - \frac{L_S J_{z0} \eta_0}{L_Z B_z \Delta_Z}\right) \end{vmatrix} = 0 . \qquad (40)$$

Equation (40) represents a balance between the radiation enhanced gradient "sources" and the parallel flow "sinks".

The solution of Eq.(40) for the turbulent saturated state is represented in terms of a nonlinear algebraic equation for the turbulent radial velocity,

$$\frac{v_r}{v_{r0}} = 1 + \eta_Z \left[1 + \left(\Gamma_Z - \Gamma_R\right)\left(\frac{v_r}{v_{r0}}\right)^{-2/3} \right] + \Gamma_R \left(\frac{v_r}{v_{r0}}\right)^{1/3} , \qquad (41)$$

where v_{r0} is the turbulent radial velocity for a model with only a Spitzer resistivity gradient, without impurity gradient and radiation enhancement,

$$v_{r0} = \frac{L_S J_{z0} \eta_0}{L_\eta B_z} . \qquad (42)$$

Here, the radiation rate parameters are:

$$\Gamma_R = \frac{\gamma_R}{\bar{\gamma}_R} , \quad \Gamma_Z = \frac{\gamma_Z}{\bar{\gamma}_Z} , \qquad (43)$$

$$\bar{\gamma}_R = \left(\frac{L_S J_{z0} \eta_0}{L_\eta B_z}\right)^{2/3} \left(\chi_T k_{\|}'^2\right)^{1/3} , \text{ and } \bar{\gamma}_Z = \bar{\gamma}_R \left(\frac{\chi_Z}{\chi_T}\right)^{1/3} . \qquad (44)$$

It should be noted that typically $\Gamma_Z > \Gamma_R$ so that the $\Gamma_Z - \Gamma_R$ term enhances the saturated state. The turbulent radial velocity, $v_{r,I_Z=0}$, in the limit of no impurity radiation enhancement, is

$$v_{r,\, I_Z=0} = v_{r0}\left(1 + \eta_Z\right) . \qquad (45)$$

From Eq. (41) for the radial velocity, all the quantities of interest can be derived. In particular, the radial diffusion coefficient and the potential fluctuation are given here. Using Eq. (35) and Eq. (41), the nonlinear algebraic equation for the turbulent resistivity diffusion coefficient at saturation is given by

$$\frac{D_T}{D_{T0}} = \left\{ 1 + \eta_Z \left[1 + \left(\Gamma_Z - \Gamma_R \right) \left(\frac{D_T}{D_{T0}} \right)^{-1/2} \right] + \Gamma_R \left(\frac{D_T}{D_{T0}} \right)^{1/4} \right\}^{4/3}, \tag{46}$$

where the diffusion coefficient for a model with only resistivity gradients is

$$D_{T0} = \left(\frac{L_S J_{z0} \eta_0}{L_\eta B_z} \right)^{4/3} \left(\chi_T k_{||}'^2 \right)^{-1/3}; \tag{47}$$

and the relation for the impurity diffusion coefficient is $D_Z = D_T (\chi_T / \chi_Z)^{1/3}$. The resistivity diffusion coefficient, $D_{T, Iz=0}$, in the limit of no impurity radiation enhancement, is

$$D_{T,\, I_{Z=0}} = D_{T0} \left(1 + \eta_Z \right)^{4/3}. \tag{48}$$

The nonlinear algebraic equation for the potential fluctuation at saturation is obtained from Eq. (41) and the average turbulent radial velocity definition,

$$\frac{\left(\frac{e\Phi}{T_e} \right)}{\left(\frac{e\Phi}{T_e} \right)_0} = 1 + \eta_Z \left\{ 1 + \left(\Gamma_Z - \Gamma_R \right) \left[\frac{\left(\frac{e\Phi}{T_e} \right)}{\left(\frac{e\Phi}{T_e} \right)_0} \right]^{2/3} \right\} + \Gamma_R \left[\frac{\left(\frac{e\Phi}{T_e} \right)}{\left(\frac{e\Phi}{T_e} \right)_0} \right]^{1/3}, \tag{49}$$

where the fluctuation amplitude for a model with only a resistivity gradient is

$$\left(\frac{e\Phi}{T_e} \right)_0 = \frac{L_S J_{z0} \eta_0 r_S}{L_\eta B_z c_S \rho_S m}. \tag{50}$$

Here, the sound speed is $c_S = (T_e / m_i)^{1/2}$, the gyroradius is $\rho_S = c_S / \omega_{ci}$, and the

gyrofrequency is $\omega_{ci}=eB/m_ic$. In order to fully understand the nature of the saturated state solution for the electrostatic potential fluctuations, it is useful to derive several limiting forms of Eq. (49). In the limit of no radiation rates ($\gamma_R,\gamma_Z\rightarrow 0$), the fluctuation level at saturation, $(e\Phi/T_e)_{Iz=0}$, has the simple form, with addition of resistivity and impurity gradients,

$$\left(\frac{e\Phi}{T_e}\right)_{I_Z=0}=\left(\frac{e\Phi}{T_e}\right)_0\left(1+\eta_Z\right)=\frac{L_S J_{z0}\eta_0 r_S}{B_z c_S \rho_S m}\left(\frac{1}{L_\eta}+\frac{1}{L_Z}\right). \tag{51}$$

In the limit of no impurity gradient ($\eta_Z\rightarrow 0$) and a large radiation rate ($\gamma_R\rightarrow$ large), Eq. (49) becomes

$$\left(\frac{e\Phi}{T_e}\right)=\left(\frac{e\Phi}{T_e}\right)_0\Gamma_R^{3/2}=\frac{\gamma_R^{3/2}r_S}{c_S\rho_S m}\left(\chi_T k_\parallel^{'2}\right)^{-1/2}. \tag{52}$$

A primary objective of an edge turbulence theory is to obtain particle transport coefficients. To this end, we incorporate the particle continuity equation in our analysis,

$$\left(\frac{d}{dt}+\chi_Z k_\parallel^{'2}x^2\right)\frac{\tilde{n}}{n_0}=-\tilde{v}_{rk}\frac{1}{n_0}\frac{dn_0}{dr}. \tag{53}$$

This ion density equation has been derived[15] in the same manner as the Z_{eff} equation, Eq. (7), where the compression term is obtained from a balance between the parallel ion pressure gradient and the ion-impurity friction. The nonlinear scale length for the density fluctuation is Δ_Z, and the saturation level is

$$\frac{n}{n_0}=\frac{v_r}{\chi_Z k_\parallel^{'2}\Delta_Z^2 L_n}, \tag{54}$$

where the density scale length is $L_n=[d(\ln n_0)/dr]^{-1}$. The nonlinear algebraic equation for the density fluctuation at saturation is then

$$\frac{\left(\frac{n}{n_0}\right)}{\left(\frac{n}{n_0}\right)_0} = \left\{ 1+\eta_Z \left\{ 1+\left(\Gamma_Z-\Gamma_R\right)\left[\frac{\left(\frac{n}{n_0}\right)}{\left(\frac{n}{n_0}\right)_0}\right]^{-2} \right\} + \Gamma_R \left[\frac{\left(\frac{n}{n_0}\right)}{\left(\frac{n}{n_0}\right)_0}\right] \right\}^{1/3}, \tag{55}$$

where the density fluctuation for a model with only a resistivity gradient is

$$\left(\frac{n}{n_0}\right)_0 = \frac{1}{L_n}\left(\frac{L_S J_{z0}\eta_0}{L_\eta B_z}\right)^{1/3}\left(\chi_Z k_{||}^{'2}\right)^{1/3}. \tag{56}$$

The density fluctuation , $(n/n_0)_{Iz=0}$, in the limit of no impurity radiation enhancement is

$$\left(\frac{n}{n_0}\right)_{I_Z=0} = \left(\frac{n}{n_0}\right)_0 \left(1+\eta_Z\right)^{1/3}. \tag{57}$$

The radial particle turbulent diffusion at saturation is derived from Eq. (55), the particle flux relation, $\Gamma_n=n_0 v_r(n/n_0)$, and the diffusion relation, $D_n=L_n\Gamma_n/n_0$,

$$\frac{D_n}{D_{n0}} = \left\{ 1+\eta_Z\left[1+\left(\Gamma_Z-\Gamma_R\right)\left(\frac{D_n}{D_{n0}}\right)^{-1/2}\right] + \Gamma_R\left(\frac{D_n}{D_{n0}}\right)^{1/4} \right\}^{4/3}, \tag{58}$$

where the diffusion coefficient for a model with only a resistivity gradient is

$$D_{n0} = \left(\frac{L_S J_{z0}\eta_0}{L_\eta B_z}\right)^{4/3}\left(\chi_Z k_{||}^{'2}\right)^{-1/3}. \tag{59}$$

It is instructive to take several limits of the expression for the particle diffusion coefficient at saturation, Eq. (58), in order to analyze the scaling of the result with the parallel conduction saturation. In the limit of no radiation rates ($\gamma_R, \gamma_Z \rightarrow 0$), the particle diffusion coefficient, $D_{n,Iz=0}$, becomes

$$D_{n,I_Z=0} = D_{n0}\left(1+\eta_Z\right)^{4/\beta} = \left[\frac{L_S J_{z0}\eta_0}{B_Z}\left(\frac{1}{L_\eta}+\frac{1}{L_Z}\right)\right]^{4/3}\left(\chi_Z k_{||}^{'2}\right)^{-1/3}, \tag{60}$$

which is a simple result with an additive resistivity and impurity gradient. In the limit of no impurity gradient ($\eta_Z \rightarrow 0$) and a large radiation rate ($\gamma_R \rightarrow$ large), Eq. (58) reduces to

$$D_n = D_{n0}\Gamma_R^2 = \gamma_R^2\left(\frac{\chi_Z}{\chi_T}\right)^{2/3}\left(\chi_Z k_{\|}'^2\right)^{-1}, \tag{61}$$

which indicates a strong scaling with the parallel conduction damping. It should be noted that this radiation dominated limit, $D \rightarrow \gamma_R{}^2 L_S{}^2/\chi k_\theta{}^2$, is precisely that which was obtained in the heuristic section, Eq.(14). From Eq. (61) it is clear that the particle diffusion coefficent has a reduces sensitivity to a scaling with the loop voltage (V_L, $E_0 \sim V_L/2\pi R_0$). In the limit of $\Gamma_Z >> \Gamma_R$, $\Gamma_Z >> 1$, $\eta_Z\Gamma_Z >> \Gamma_R$, and $\eta_Z\Gamma_Z >> 1$, Eq. (58) becomes

$$D_n = D_{n0}\left(\eta_Z\Gamma_Z\right)^{4/5} = \left(\frac{L_S J_{z0}\eta_0}{L_Z B_z}\right)^{4/5}\gamma_Z^{4/5}\left(\frac{\chi_Z}{\chi_T}\right)^{-1/3}\left(\chi_Z k_{\|}'^2\right)^{-3/5}, \tag{62}$$

which also indicates a strong scaling of the saturation with parallel conduction damping. Consequently, the saturation results indicate that the parallel conduction quenches the thermal instability and imposes a clearcut limit on the level of turbulence at saturation. In general, the impurity radiation enhances the saturation level of the resistivity-impurity gradient driven turbulence; however, the resistivity-impurity gradient driven turbulence tends to regulate the thermal instability. We also conclude that the impurity radiation enhancement of the fluctuation levels at saturation might be responsible for the observed particle confinement time (τ_p) roll-over[6] at high density (n).

Magnetic fluctuations, B_r/B_z, are also produced along with the electrostatic ones which we have primarily addressed. Here, we follow the approximate calculation of the magnetic fluctuations given in Ref. 15. The tearing parity component of the fluctuation is calculated using the constant-ψ approximation. The magnetic fluctuation in terms of the radial scales is

$$\frac{B_r}{B_z} \cong \frac{\mu_0 J_{z0}}{2B_z}\left(\frac{\Delta_T^2}{L_\eta}+\frac{\Delta_Z^2}{L_Z}\right). \tag{63}$$

Using Eqs. (34) and (41), the magnetic fluctuation can be evaluated in terms of the electrostatic potential fluctuation,

$$\frac{B_r}{B_z}=\frac{\mu_0 J_{z0}}{2B_z L_\eta}\left(\frac{c_S \rho_S r_S L_S^2}{m\chi_T}\right)^{2/3}\left[1+\eta_Z\left(\frac{\chi_T}{\chi_Z}\right)^{2/3}\right]\left(\frac{e\Phi}{T_e}\right)^{2/3}. \tag{64}$$

The thermal conduction induced by the magnetic fluctuations can be estimated by $\chi_\perp \cong \chi_T (B_r/B_z)^2$.

Evaluations of the above saturation expressions have been compared for a typical low density tokamak (Text) and a typical high density tokamak (Alcator). The machine edge parameters are listed in Table I. The derived parameters are listed in Table II. Besides the adoption of well known formulas for several derived parameters (taken from the NRL plasma formulary), a simple quadratic $q(r)$ profile has been assumed. The impurity radiation rate parameters have been obtained (for a carbon impurity) assuming a coronal equilibrium.[24] In the temperature range of interest for the edge plasma, the ionization state is C-IV (as noted in the atomic data tables, Ref. 24). The impurity density is assumed to be roughly 1% of the edge density. The fluctuation levels, with no impurity radiation ($I_Z=0$), are listed at the bottom of Table III. The linear and nonlinear saturated state results for the typical machine parameters are listed in Table IV. A comparison of the impurity radiation enhancement results for several edge temperatures (20eV, 15eV, and 10eV) are displayed in Table V. For the case of a low edge temperature (10eV), the radiation enhancement of the saturation values is sizeable for the high density machine (greater than an order of magnitude for Alcator). However, there is only a small effect for the low density machine.

The linear growth rates, nonlinear saturation fluctuation levels, and transport coefficients are extremely sensitive to the particular machine operating parameters considered. Slight increases in the impurity radiation rate can drastically boost the results. Consequently, it is instructive to determine all the results as a function of the

radiation rate. It should be noted that the larger radiation rates considered (above our "typical" values) can be realized by considering a lower edge temperature, a larger impurity edge density, and an improved noncoronal radiation rate model. The linear eigenfunction is presented in Fig. 1(a) for the typical Text parameters. A comparison of the eigenfunction for an assumed large radiation rate (with Text parameters), Fig 1(b), indicates a very similar structure. The enhancement of the growth rate (for Text parameters) versus a normalized radiation rate is shown in Fig. 2, which indicates a linear dependence. A comparison between the electrostatic potential fluctuation and the density fluctuation at saturation (for Text parameters) versus the normalized radiation rate is shown in Fig. 3. For low impurity radiation rates, the density fluctuation is greater than the potential fluctuation. However, for higher radiation rates, the potential fluctuation is significantly greater than the density fluctuation. In fact, the nonlinear structure responsible for the impurity radiation enhancement of the potential and density fluctuations tends to force the potential fluctuation greater than the density fluctuation at saturation ($e\Phi/T_e > n/n_0$), which is in agreement with experiment[4]. The disparity in enhancement scaling for the density and potential fluctuations can be understood by noting from Eq. (54) that the density fluctuations are weak functions of the diffusion coefficient ($n/n_0 \sim \Delta/L \sim D^{1/4}$), whereas the potential fluctuations are strongly dependent on the diffusion coefficient ($e\Phi/T_e \sim D^{3/4}$). It should be noted that we refer to the plasma edge as the region just before the limiter where the potential fluctuations are significantly larger than the density fluctuations and the impurity radiation tends to peak. This is in contrast to the scrape-off-layer region (just beyond the limiter) where the density fluctuations are above the potential fluctuations. Finally, the particle diffusion coefficient and the magnetic induced thermal conductivity are displayed in Fig. 4 as a function of the normalized impurity radiation rate (for Text parameters). The thermal conduction is over two orders of magnitude smaller than the particle diffusion coefficient. Typically, the impurity radiation enhancement results in diffusion coefficients on the order of experiment ($D_n > 10^4 cm^2/sec$).

VI. DISCUSSION AND SUMMARY

The linear and nonlinear theory for thermally driven convective cells and tokamak edge turbulence has been presented in detail. The analysis involved a coupling of the thermal instability with resistivity-impurity gradient driven turbulence. It was noted that the turbulently elevated cross-field transport is essential for a satisfactory model of saturated state parallel conduction damping (which regulates the thermal instability). The basic result of this analysis is that the impurity radiation cooling enhances the fluctuation saturation levels and thus enhances the transport coefficients, while the thermally driven convective cell turbulence in turn regulates the thermal instability.

Results have been presented for a typical low density (Text) and a high density (Alcator) tokamak. The calculations indicate that there is sizeable enhancement (over an order of magnitude) in the nonlinear saturation levels, and transport coefficients for high density machines (such as Alcator) where the radiation rates are significant. For this regime, the turbulently elevated parallel conduction damping, when coupled with the thermal instability, alters the scaling of the saturation values. In particular, the radial particle diffusion coefficient scales as $D_n \propto (\chi_Z k_{\|}'^2)^{-1}$, which shows a strong dependence on the parallel conduction damping, so that the thermal instability is quenched and a clearcut limit on the level of turbulence at saturation is imposed. The detailed result demonstrates that there is a smooth connection from weak impurity radiation conditions to radiation dominated situations which indicate that the particle diffusion coefficent has a reduces sensitivity to a scaling with the loop voltage ($V_L, E_0 \sim V_L/2\pi R_0$). Also, the calculated fluctuation amplitudes and the particle diffusion coefficients ($D_n > 10^4 cm^2/sec$) are found to be on the order of experimental values. Since the impurity radiation effect has been shown to be significant, it has been proposed that the impurity radiation enhancement of the fluctuation levels at saturation might be responsible for the observed particle confinement time (τ_p) roll-over[6] at high density (n).

The saturation fluctuation levels are found to be sensitive to the particular operating parameters considered. Consequently, for Text parameters, the results have also been displayed as functions of the radiation rate. The linear eigenmodes

are found to have the same structure for a low or a high radiation rate. For large radiation rates, the linear growth rate is linearly dependent on the radiation rate. The particle diffusion coefficient is qualitatively linear in the radiation rate, while the magnetic fluctuation induced radial conductivity approximately tracks this dependence, but with an amplitude that is two orders of magnitude lower. The electrostatic potential fluctuation amplitude is also roughly linearly dependent on the radiation rate; however, the density fluctuation amplitude is weakly dependent on the radiation rate. This was understood by noting the weak scaling of the density ($n/n_0 \sim \Delta/L \sim D^{1/4}$) and the strong scaling of the potential fluctuations with the diffusion coefficient ($e\Phi/T_e \sim D^{3/4}$). Consequently, the thermally driven convective cell turbulence theory indicates the significant result that the nonlinear structure responsible for the impurity radiation enhancement of the potential and density fluctuations tends to force the potential fluctuation greater than the density fluctuation at saturation ($e\Phi/T_e > n/n_0$), which is in agreement with experiment[4].

Future work on this subject will include comparisons between theory and experiment when one takes into account the detailed profile information from various machines. We also plan to extend this work by including an ionization source with recycling, which will drive density fluctuations, and therefore will couple to drift wave turbulence. This should prove relevant in an understanding of the improved confinement for the H-mode and supershot, where the ionization is observed to be low.

ACKNOWLEDGMENTS

We would like to acknowledge fruitful discussions with A. J. Wootton, B. A. Carreras, P. W. Terry, T. S. Hahm, and J. F. Drake.

This research was supported by the U.S. Department of Energy Contract No. DE-FG05-80ET-53088.

REFERENCES

1. C. M. Surko and R. E. Slusher, Science **221**, 817 (1983).
2. S. J. Zweben and R. W. Gould, Nucl. Fusion **23**, 1625 (1983).
3. S. J. Levinson, J. M. Beall, E. J. Powers, and R. D. Bengtson, Nucl. Fusion **24**, 527 (1984).
4. Ch. P. Ritz, R. D. Bengtson, S. J. Levinson, and E. J. Powers, Phys. Fluids **27**, 2956 (1984).
5. A. J. Wootton, H. Howe, P. H. Edmonds, C. H. Ma, P. K. Mioduszewki, and K. Yokoyama, submitted to Nucl. Fusion.
6. W. L. Rowan, C. C. Klepper, Ch. P. Ritz, R. D. Bengtson, K. W. Gentle, P. E. Phillips, T. L. Rhodes, B. Richards, and A. J. Wootton, accepted for publication in Nucl. Fusion.
7. F. Wagner, *et al.*, Phys. Rev. Lett. **53**, 1453 (1984).
8. J. D. Callen, B. A. Carreras, P. H. Diamond, M. E. Benchikh-Lehocine, L. Garcia, and H. R. Hicks, in *Plasma Physics and Controlled Nuclear Fusion Research, 1982* (IAEA, Vienna, 1983), Vol. 1, p. 297.
9. P. W. Terry, and P. H. Diamond, Phys. Fluids **28**, 1419 (1985).
10. H. P. Furth, J. Killeen, and M. N. Rosenbluth, Phys. Fluids **6**, 459 (1963).
11. L. Garcia, P. H. Diamond, B. A. Carreras, and J. D. Callen, Phys. Fluids **28**, 2147 (1985).
12. B. A. Carreras, P. W. Gaffney, H. R. Hicks, and J. D. Callen, Phys. Fluids **26**, 1231 (1982).
13. P. W. Terry, P. H. Diamond, K. C. Shaing, L. Garcia, and B. A. Carreras, Phys. Fluids **29**, 2501 (1986).
14. P. H. Rutherford, in *Physics of Plasma Close to Thermonuclear Conditions*, edited by B. Coppi *et al.* (Pergamon, New York, 1981), Vol. I, p. 143.
15. T. S. Hahm, P. H. Diamond, P. W. Terry, L. Garcia, and B. A. Carreras, Phys. Fluids **30**, 1452 (1987).
16. B. B. Kadomtsev and O. P. Pogutse, in *Reviews of Plasma Physics*, edited by M. Leontovich (Consultants Bureau, New York, 1970), Vol. V, p. 349.
17. D. R. Thayer, P. H. Diamond, and A. J. Wootton, J. Nucl. Mat. **145**, 803 (1987).
18. B. Lipschultz, B. LaBombard, E. S. Marmar, M. M. Pickrell, J. L. Terry, R. Watterson, and S. M. Wolfe, Nucl. Fusion **24**, 977 (1984).
19. J. D. Strachan, *et al.*, J. Nucl. Mat. **145**, 186 (1987).

20. T. E. Stringer, in *12th European Conference on Controlled Fusion and Plasma Physics* , (Budapest, Hungary, 1985), Part I, p. 86.
21. J. Neuhauser, W. Schneider, and R. O. Wunderlick, Max-Planck-Institut fur Plasmaphysik, Garching Rep. #IPP5/8 (1985).
22. J. F. Drake, Laboratory for Plasma Fusion Energy Studies, University of Maryland, College Park, MD, Rep. UMLPF #87-020 (1986).
23. H. R. Strauss, Phys. Fluids **19**, 134 (1976).
24. D. E. Post, *et al.*, Atomic Data Tables **20**, 397 (1977).

FIGURE CAPTIONS

Fig. 1 The normalized linear eigenmode, ϕ/ϕ_0, (from a shooting code solution) versus the normalized coordinate about the mode rational surface, x/x_R, for (a) Text parameters, and (b) Text parameters with an enhanced radiation rate $I_Z=10I_{Z0}$, for $I_{Z0}=20I_Z(T_0=15eV)$.

Fig. 2 The normalized linear growth rate, $\gamma/\gamma_{Iz=0}$, for Text parameters versus a normalized radiation rate, I_Z/I_{Z0}, for $I_{Z0}=20I_Z(T_0=15eV)$.

Fig. 3 The normalized electrostatic potential fluctuation amplitude, $e\Phi/T_e$, and the normalized density fluctuation amplitude, n/n_0, for Text parameters versus a normalized radiation rate, I_Z/I_{Z0}, for $I_{Z0}=20I_Z(T_0=15eV)$.

Fig. 4 The radial particle diffusion coefficient, D_n, and the magnetic fluctuation induced radial conduction times 100, $10^2\chi_\perp$, (in units of m^2/sec) for Text parameters versus a normalized radiation rate, I_Z/I_{Z0}, for $I_{Z0}=20I_Z(T_0=15eV)$.

TABLE CAPTIONS

Table I. Machine parameters.

Table II. Derived parameters.

Table III. Resultant parameters used in the saturation calculations.

Table IV. Linear and nonlinear saturation enhanced results.

Table V. Enhancement of turbulence levels for (a) T_0=20eV with $I_z/T_0=2.4\times10^{-16}m^3/sec$ and $-dI_z/dT_0=4.3\times10^{-16}m^3/sec$, (b) T_0=15eV with $I_z/T_0=1.2\times10^{-15}m^3/sec$ and $-dI_z/dT_0=8.0\times10^{-15}m^3/sec$, and (c) T_0=10eV with $I_z/T_0=2.1\times10^{-14}m^3/sec$ and $-dI_z/dT_0=9.5\times10^{-14}m^3/sec$.

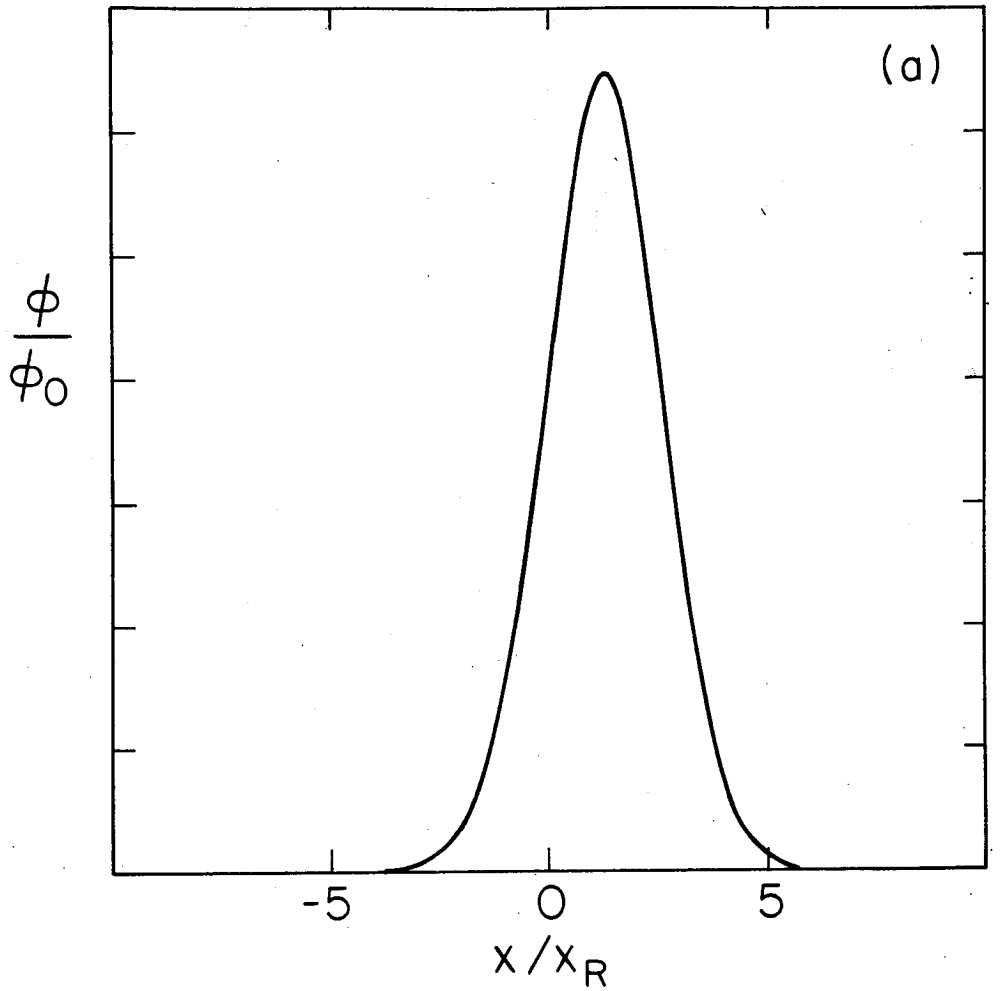

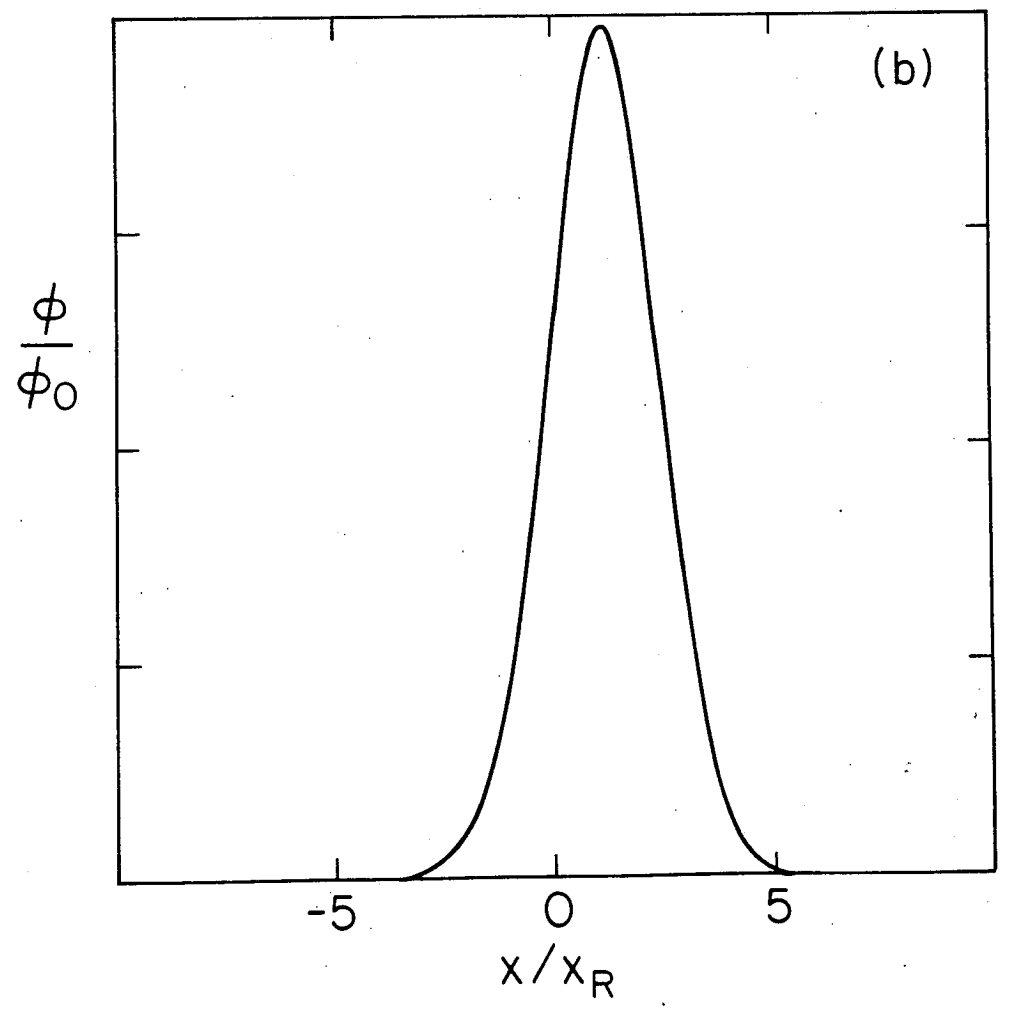

Fig. 1

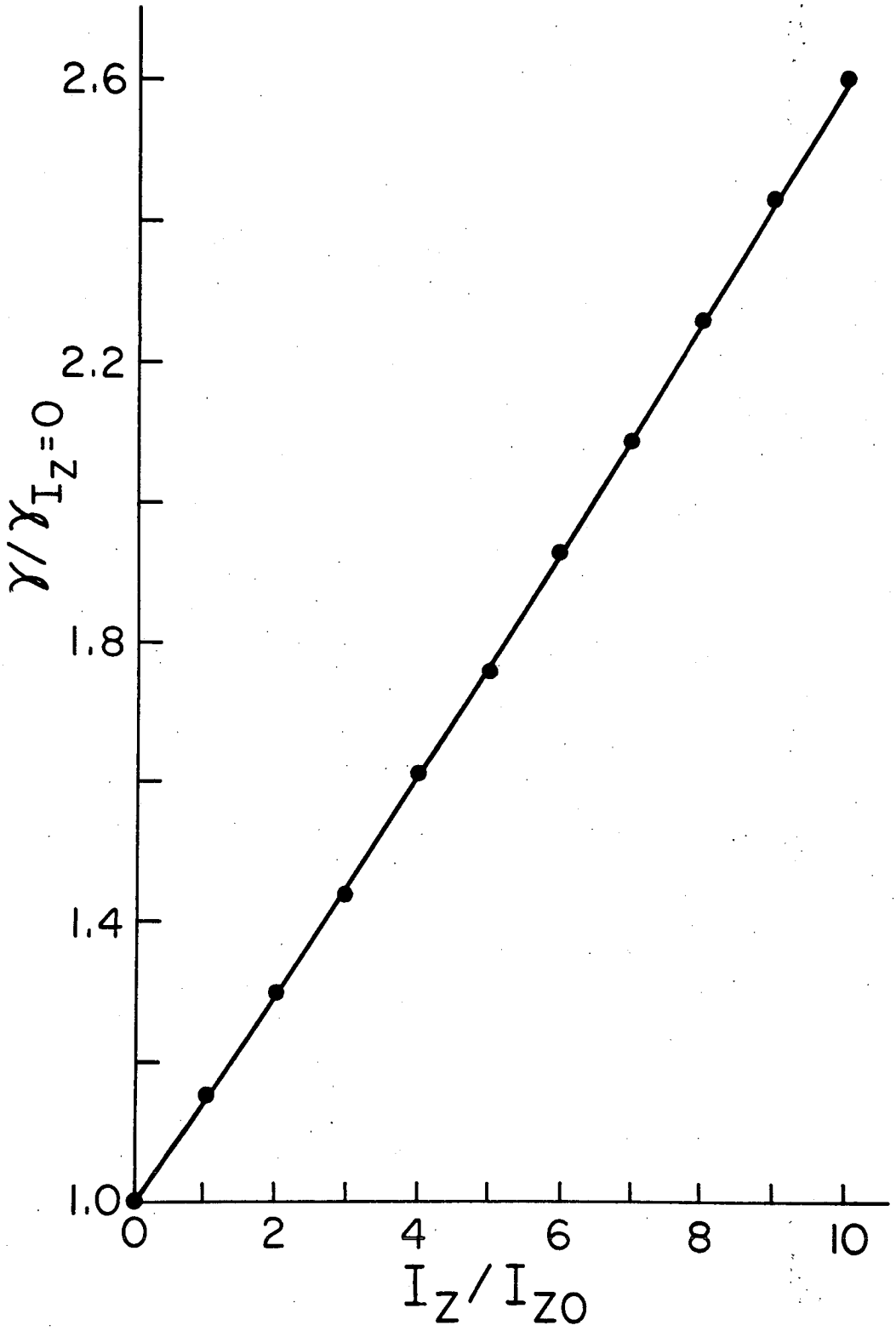

Fig. 2

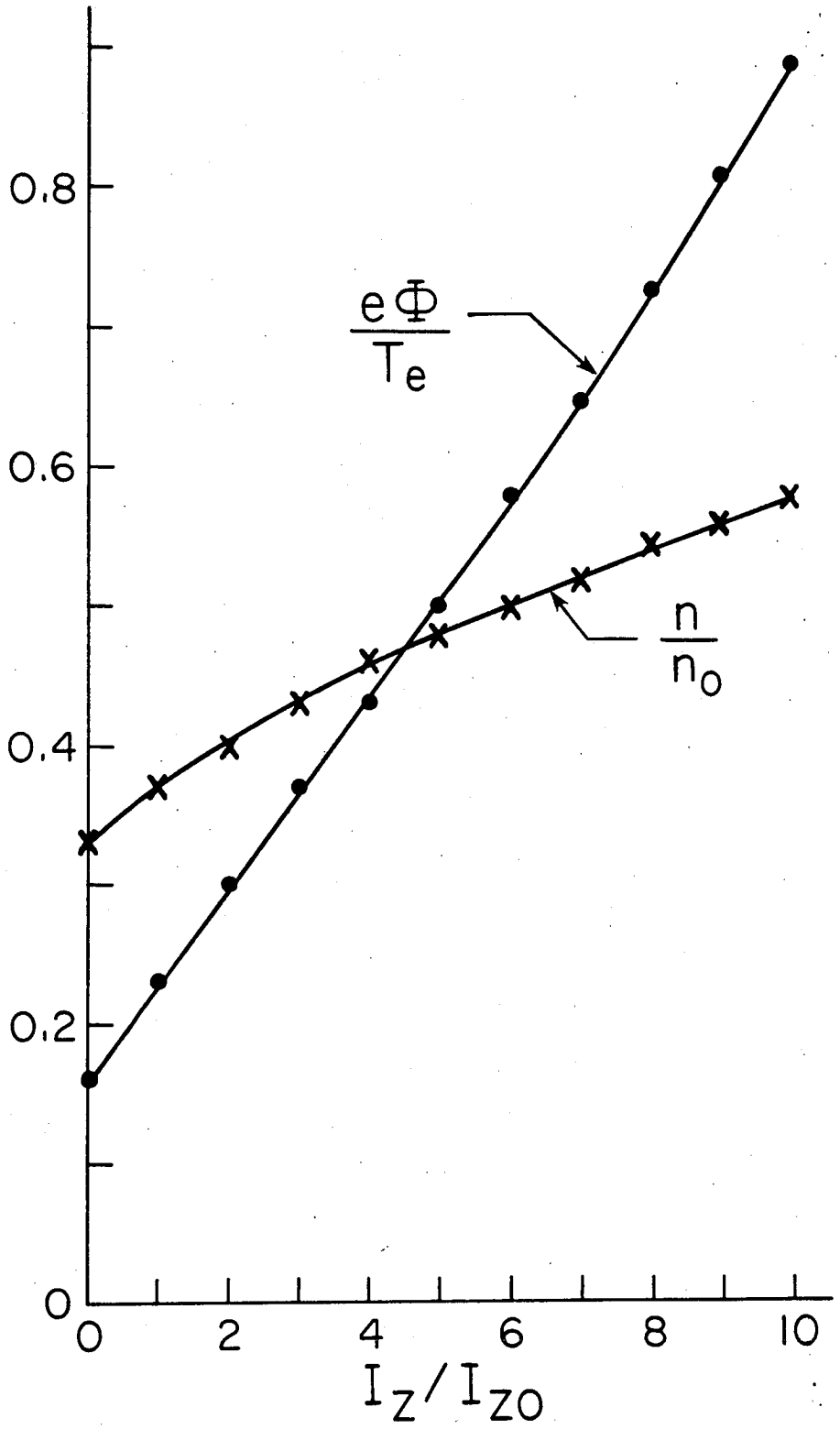

Fig. 3

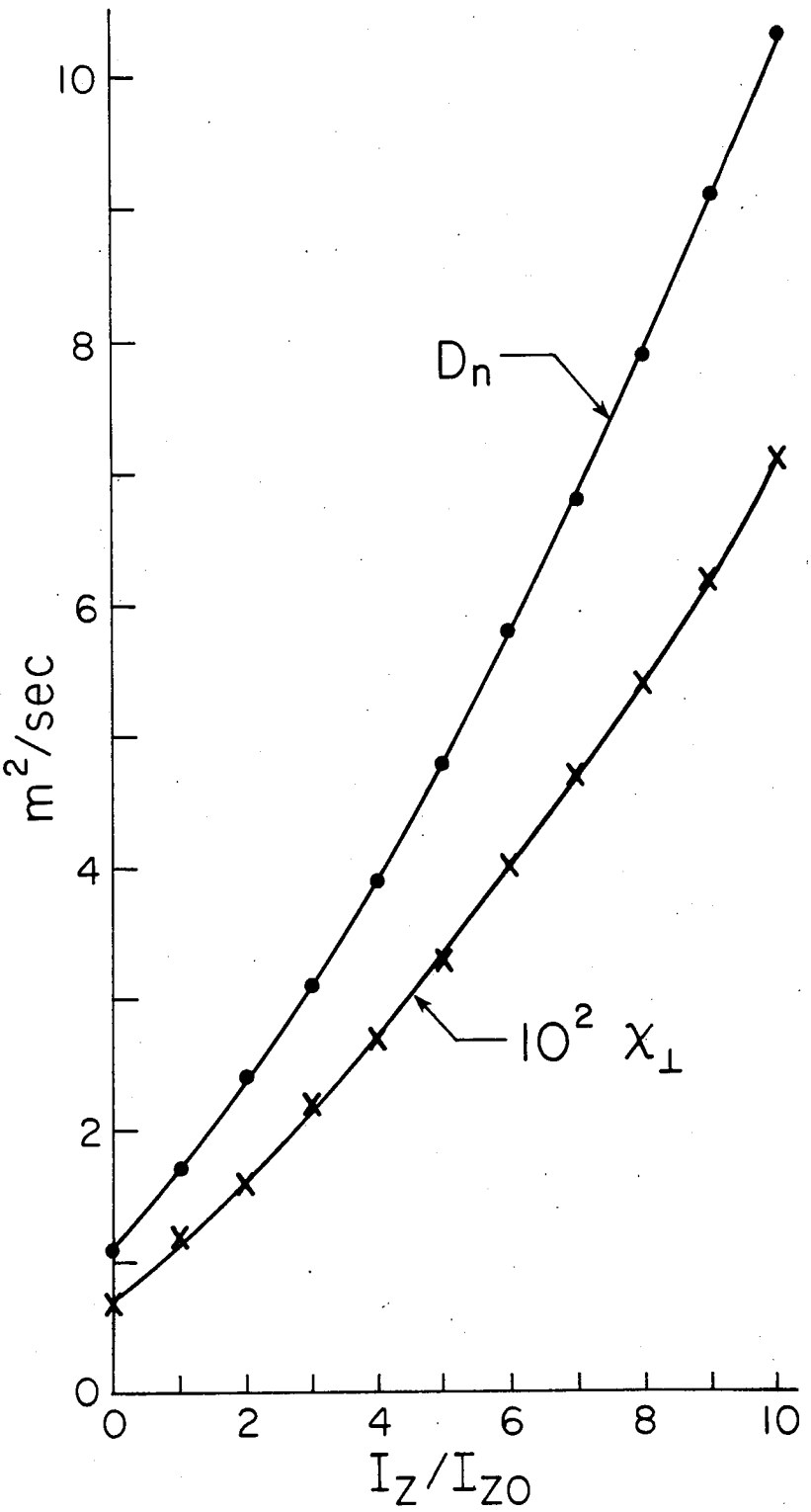

Fig. 4

	Text	Alcator
a, m	0.26	0.165
R_0, m	1.0	0.64
T_0, eV	15.0	15.0
B_z, T	2.0	13.0
I, A	2.0×10^5	8.0×10^5
n_0, m^{-3}	8.0×10^{18}	2.0×10^{20}
$q(0)$, m	1.0	1.0
L_η, m	0.05	0.05
L_η / L_n	2.0	2.0
Z_{eff}	1.2	1.2
η_z	0.5	0.5
m	22.0	22.0
n	7.0	7.0

Table I

	Text	Alcator
r_s , m	0.21	0.13
L_s , m	1.1	0.69
$\ln\Lambda$	12.0	10.0
η_0/μ_0, m^2/sec	20.0	17.0
$\mu_0 J_{z0}/B_z$, m^{-1}	0.20	0.32
χ_T, m^2/sec	1.2×10^6	5.5×10^4
χ_z/χ_T	0.020	0.020
c_s, m/sec	3.8×10^4	3.8×10^4
ρ_s, m	2.0×10^{-4}	3.0×10^{-5}
n_{z0}/n_0	0.013	0.013
I_z/T_0, m^3/sec	1.2×10^{-15}	1.2×10^{-15}
$-dI_z/dT_0$, m^3/sec	8.0×10^{-15}	8.0×10^{-15}
Z	4.0	4.0
γ_R, sec^{-1}	6.1×10^2	1.5×10^4
γ_z, sec^{-1}	7.2×10^2	1.8×10^4

Table II

	Text	Alcator
γ_0, sec^{-1}	5.3×10^4	7.8×10^4
x_{RO}, m	5.8×10^{-4}	3.4×10^{-4}
γ_R/γ_0	0.012	0.20
γ_Z/γ_0	0.014	0.23
$\bar{\gamma}_R$, sec^{-1}	4.4×10^4	2.7×10^4
$\bar{\gamma}_Z$, sec^{-1}	1.2×10^4	7.2×10^3
Γ_R	0.014	0.58
Γ_Z	0.060	2.5
$(e\Phi/T_e)_{I_Z=0}$	0.16	0.58
$(n/n_0)_{I_Z=0}$	0.33	0.48
$D_{n,I=0}$, m^2/sec	1.1	1.3
$(B_r/B_Z)_{I_Z=0}$	7.9×10^{-5}	2.6×10^{-4}

Table III

	Text	Alcator
$\gamma/\gamma_{I_z=0}$	1.0	1.1
$\left(\frac{e\Phi}{T_e}\right)/\left(\frac{e\Phi}{T_e}\right)_{I_z=0}$	1.0	1.9
$\left(\frac{n}{n_o}\right)/\left(\frac{n}{n_o}\right)_{I_z=0}$	1.0	1.2
$\left(\frac{B_r}{B_z}\right)/\left(\frac{B_r}{B_z}\right)_{I_z=0}$	1.0	1.5
$D_n/D_{n,I_z=0}$	1.0	2.3
γ, sec^{-1}	6.5×10^4	1.2×10^5
$e\Phi/T_e$	0.17	1.1
n/n_o	0.33	0.59
B_r/B_z	8.0×10^{-5}	3.9×10^{-4}
D_n, m^2/sec	1.1	3.1
$\chi_\perp$, m/sec	7.7×10^{-3}	8.3×10^{-3}

Table IV

(a)

	Low Density (Text)	High Density (Alcator)
$\gamma/\gamma_{I_z=0}$	1.0	1.0
$\left(\frac{e\Phi}{T_e}\right)/\left(\frac{e\Phi}{T_e}\right)_{I_z=0}$	1.0	1.1
$\left(\frac{n}{n_o}\right)/\left(\frac{n}{n_o}\right)_{I_z=0}$	1.0	1.0
$D_n/D_{n,I_z=0}$	1.0	1.2

(b)

	Low Density (Text)	High Density (Alcator)
$\gamma/\gamma_{I_z=0}$	1.0	1.1
$\left(\frac{e\Phi}{T_e}\right)/\left(\frac{e\Phi}{T_e}\right)_{I_z=0}$	1.0	1.9
$\left(\frac{n}{n_o}\right)/\left(\frac{n}{n_o}\right)_{I_z=0}$	1.0	1.2
$D_n/D_{n,I_z=0}$	1.0	2.3

(c)

	Low Density (Text)	High Density (Alcator)
$\gamma/\gamma_{I_z=0}$	1.1	2.2
$\left(\frac{e\Phi}{T_e}\right)/\left(\frac{e\Phi}{T_e}\right)_{I_z=0}$	1.3	16.0
$\left(\frac{n}{n_o}\right)/\left(\frac{n}{n_o}\right)_{I_z=0}$	1.1	2.5
$D_n/D_{n,I_z=0}$	1.4	39.0

Table V